CHAPTER VI

GENERATION OF $(ZnH_3)^+$ SPECIES OVER HYDROGEN–TREATED Zn/HZSM–5 CATALYSTS FOR *n*–PENTANE AROMATIZATION

(Submitted to Journal of Molecular Catalysis A: Chemical)

6.1 Abstract

The effects of hydrogen treatment on Zn/HZSM–5 catalysts to the evolution of zinc species and their activity in *n*–pentane aromatization were studied. By heating Zn/HZSM–5 catalysts under inert atmosphere, most of zinc species appeared as $(ZnOH)^+$. The XPS and IPA–TPD results showed that using H_2 as a treatment gas, the hydrodehydroxylation of $(ZnOH)^+$ generated $(ZnH)^+$ species with the recovery of some Brønsted acid sites. It was found that under the hydrogen atmosphere, the H_2 molecule was dissociated on this Zn species and generated the active $(ZnH_3)^+$ species. Compared with HZSM–5 catalyst, the presence of $(ZnOH)^+$ species improved the aromatics selectivity from 11 % to 22 %. Nevertheless, after pre–treating Zn/HZSM–5 with H_2, the formation of $(ZnH_3)^+$ species remarkably increased the BTX aromatics selectivity to 31 %. It was found that the $(ZnH_3)^+$ species was not stable due to the recombinative desorption of hydrogen from $(ZnH_3)^+$ species recovered the $(ZnH)^+$ species. However the $(ZnH_3)^+$ species could be regenerated by H_2 treatment.

Keywords: Zn/HZSM–5, $(ZnOH)^+$, $(ZnH)^+$, Pentane, Brønsted acid, Aromatics

6.2 Introduction

Due to the large volume of light paraffinic hydrocarbons, contained in associated gas and a considerable amount of light naphtha components (*n*–C_5H_{12} and *n*–C_6H_{14}), derived from petroleum refining process, the catalytic conversion of light hydrocarbons to more valuable chemicals has gained more attention [1-7]. One of the most promising pathways is the transformation of light naphtha to benzene, toluene, and xylenes (BTX aromatics), important aromatic building blocks in the

petrochemical industry. It is known that the HZSM–5 structure provides a great performance in both aromatics selectivity and stability for the conversion of light alkanes to aromatics. Moreover, its activity and selectivity can be enhanced by introducing dehydrogenation promoters such as platinum, gallium or zinc [8-10].

Zn–exchanged HZSM–5 was found to be one of the most efficient catalysts for the dehydrogenation and aromatization of light alkanes [10-17]. The reaction mechanism involves a complicated acid–catalyzed reaction. While Zn cations enhance the dehydrogenation ability, the Brønsted acid sites are responsible for the catalytic cracking of paraffins and also the oligomerization and aromatization of the olefins [18, 19]. The remarkably high activity in alkane dehydrogenation of Zn cations comes from the high performance in dissociative adsorption, recombination, and desorption processes of hydrogen [1, 10, 18, 20-24].

Summarizing the results from previous theoretical and experimental studies, one can conclude that Zn species are strongly depended on the preparation methods. Using aqueous phase ion exchange method, only $(ZnOH)^+$ at isolated Al center were formed. When this species locates in a proximity with another Brønsted acid site, the $(ZnOH)^+$ was found to be unstable at high temperature and tend to form Zn^{2+} in the vicinity of the two Al centers [25]. However, at high Si/Al ratios, the possibility that two Al ions locating at the same ring of the zeolite framework is very low, thus most Zn species was reported to appear as $(ZnOH)^+$ species. It is broadly believed that this Zn species are responsible for the enhancement of aromatics yield over Zn/HZSM–5 catalyst due to its ability for both H_2 dissociation and recombinative desorption [26, 27]. Although the Zn cations locating at the exchangeable site cannot be completely reduced even at 900 °C [18], Triwahyono and co–workers showed that heating Zn/HZSM–5 catalyst under H_2 atmosphere could generate Brønsted acid site that could enhance the isomerization of *n*–pentane. The pyridine–IR experiments suggests that this site is a reversible process and only existed in the hydrogen atmosphere [28]. Theoretical studies on hydrogen dissociation and recombination processes of zeolite Zn(II) cations have also been investigated for a decade [27, 29]. Despite that the understanding on the formation of the active zinc species upon reduction has not been reported.

In this work, the evolution of Zn species in Zn/HZSM–5 catalyst after different thermal treatments has been elucidated. Zn–containing HZSM–5 zeolite was prepared by aqueous phase ion–exchange. The Zn species, before and after thermal treatments under H_2 and inert atmospheres, was analyzed by XPS. The change in acidic properties upon such treatments was observed by IPA–TPD (temperature programmed desorption of isopropylamine). Catalytic activity of the Zn–containing HZSM–5 zeolites was investigated for the aromatization of *n*–pentane.

6.3 Experiment

6.3.1 Catalyst Preparation

The NH_4ZSM–5 zeolite with SiO_2/Al_2O_3 ratio of 30 was obtained from Zeolyst International. In order to convert to proton form, the NH_4ZSM–5 was calcined in air at 550 °C for 5 h. The Zn^{2+} was loaded on the HZSM–5 catalyst by aqueous phase ion–exchange. Briefly, the HZSM–5 (4 g) was stirred in 0.05 M $Zn(NO_3)_2$ solution (100 mL) at 70 °C for 12 h. The ion–exchanged sample was washed with excess deionized water, dried overnight at 120 °C, after that calcined at 550 °C in air for 5 h.

6.3.2 Characterization

The Zn loading on HZSM–5 catalyst was determined by an atomic absorption spectroscopy (AAS). Nitrogen adsorption/desorption isotherms were measured to calculate the specific surface area and micropore volume of the catalysts, using Brunauer–Emmet–Teller (BET) method. The relative crystallinities of the HZSM–5 zeolites before and after loading Zn was analyzed by a Rigaku X–ray diffractometer (XRD) with Cu tube for generating CuKα radiation (λ = 1.5418 Å) at room temperature. A temperature programmed desorption of isopropylamine (IPA–TPD) was performed in a homemade apparatus using a quarter inch quartz tube reactor connected to an online MS detector (MKS Cirrus series 903). The catalysts were heated under the process gas (He or H_2) at 500 °C for 1 h after which IPA was pulsed with the process gas at room temperature until saturated as determined by the constant amount of detected IPA. The IPA–TPD was carried out

in the range of 30–800 °C at a heating rate of 10 °C/min. X–ray absorption near edge structure (XANES) of Zn (9659 eV) K–edge were performed at beamline 8, Synchrotron Light Research Institute (SLRI), Thailand. The samples were measured in the fluorescence mode using Ge(220) double crystal monochromator at room temperature. The data analysis was performed by Arthena version 0.9.18.2. X–ray photoelectron spectroscopy (XPS) was recorded by a Kratos Ultra X–ray photoelectron spectrometer. A monochromatic AlKα was used as an X–ray source (anode HT = 15 kV). The XPS peaks were referenced to the binding energy of C (1s) peak at 285 eV. In order to study the effects of hydrogen treatment, Zn/HZSM–5 catalysts were heated under Ar or H_2 flow at various temperatures for 1 h in an XPS catalyst reaction cell. The catalysts were then cooled down under the treated gas and then transferred to the XPS chamber for the analysis.

6.3.3 Catalytic Activity Testing

The catalytic activity was tested by using a pulse reactor. In each test, 50 mg of catalyst was packed in a ¼" O.D. Pyrex fixed–bed reactor. The catalyst was heated under flow of He at 500 °C for 1 h. After that, 0.025 mL of *n*–pentane vapor (at room temperature) was pulsed into the reactor under a He flow (180 mL/min). In order to study the effect of H_2, the catalyst was heated under H_2 atmosphere (20 mL/min) at 500 °C for 1 h and then immediately changed the carrier gas to He and pulsed *n*–pentane. The effect of hydrogen treating was repeated consecutively, denoted as experiments 3, 4, 5, and 6. The products were analyzed on–line by gas chromatography using a Shimadzu 17A–GC equipped with an HP–PLOT/Al_2O_3 "*S*" deactivated capillary column.

6.4 Results and Discussion

6.4.1 Analysis of Zn Loading and Physical Properties

As shown in Table 6.1, approximately 0.87 wt % of Zn was found on Zn/HZSM–5 catalyst. As discussed in previous work [30], the low amount of Zn loading prepared by aqueous phase ion–exchange method was due to the limited exchangeability of HZSM–5 catalysts. The BET analysis showed a slight decrease in total surface area and micropore volume. This could be due to the small amount of

highly dispersed Zn loaded. The XRD results confirmed that the MFI structure remained intact after the modification (Fig. 6.1).

Table 6.1 Analysis of Zn loadings and textural properties of HZSM–5 and Zn/HZSM–5 catalysts

Catalysts	Zn loading		S_{BET}	V_{micro}
	(wt %)	(μmol Zn/g_{cat})	(m^2/g_{cat})	(cm^3/g_{cat})
HZSM–5	0	0	389.9	0.278
Zn/HZSM–5	0.87	133.07	345.5	0.218

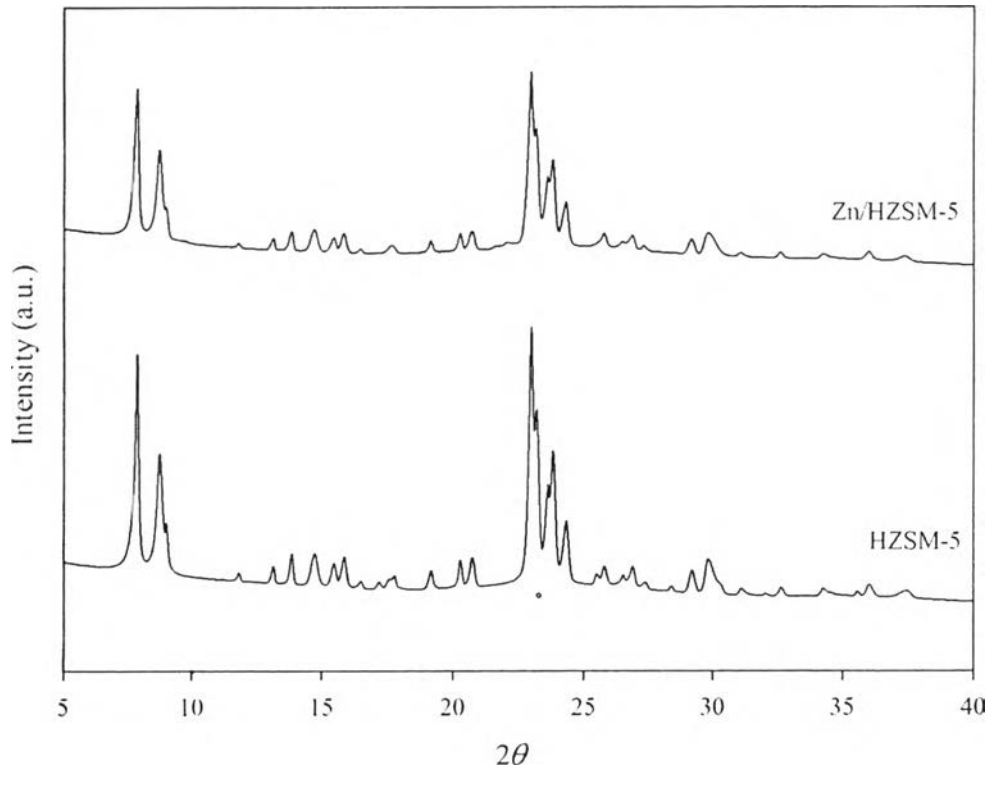

Figure 6.1 XRD patterns of HZSM–5 and Zn/HZSM–5 catalysts.

6.4.2 The Acidic Properties

The Brønsted acidic properties of parent and modified HZSM–5 catalysts were studied by a temperature programmed desorption of isopropylamine (IPA–TPD). The decomposition of isopropylamine to ammonia and propylene over Brønsted acid sites allowed us to quantify the amount of Brønsted acidity via Hofmann elimination reaction [31, 32]. As shown in Fig. 6.2, the propylene (*m/e*=41) desorbed at 350 °C was assigned to the strong Brønsted acid sites of the zeolites. After introducing Zn on HZSM–5 catalyst, the strong Brønsted acid sites significantly decreased from 373 to 189 $\mu mol/g_{cat}$ (Table 6.2). This is because cationic zinc species became counter cation for the negative framework charge [11]. Compared with HZSM–5, Zn/HZSM–5 (inert atmosphere) showed new acid sites with relatively lower acid strength at 390 °C and 480 °C [32]. These acid sites might be induced by the presence of $(ZnOH)^+$ species and part of it was formed via the hydrolysis with contaminated water in IPA. In line with previous studies on adsorption of CD_3CN, El–Malki and co–workers found the new weaker Brønsted acid sites after the hydrolysis of Zn/HZSM–5 [33]. The difference in the Brønsted acid strength was proposed to depend on the distance between $(ZnOH)^+$ species and the Brønsted acid site [34]. It was expected that the $(ZnOH)^+$ species, stabilized with a closely proximate acid site, is able to reverse between $(ZnOH)^+$ and exchangeable Zn^{2+} species. As this is a reversible process, the effect of water on this Zn^{2+} species was proposed by the hydroxylation with water molecules following equation 1.

$$2(AlO_2)^- Zn^{2+} + H_2O \rightarrow (AlO_2)^- (ZnOH)^+ + (AlO_2)^- H^+ \quad (1)$$

The effect of hydrogen to Zn/HZSM–5 catalyst was studied by heating the catalyst for one hour and performing the IPA–TPD under H_2 atmosphere. In contrast with Zn/HZSM–5 (inert atmosphere), the result showed an evolution of Brønsted acid site at 370 °C with the disappearance of the one at 390 °C and 480 °C. The change in desorbed propylene peaks illustrated that the acid site derived from the interaction with the original $(ZnOH)^+$ species was modified. It was plausibly explained that upon heating Zn/HZSM–5 catalyst under the hydrogen atmosphere, most of $(ZnOH)^+$ species performed the hydrodehydroxylation with the H_2.

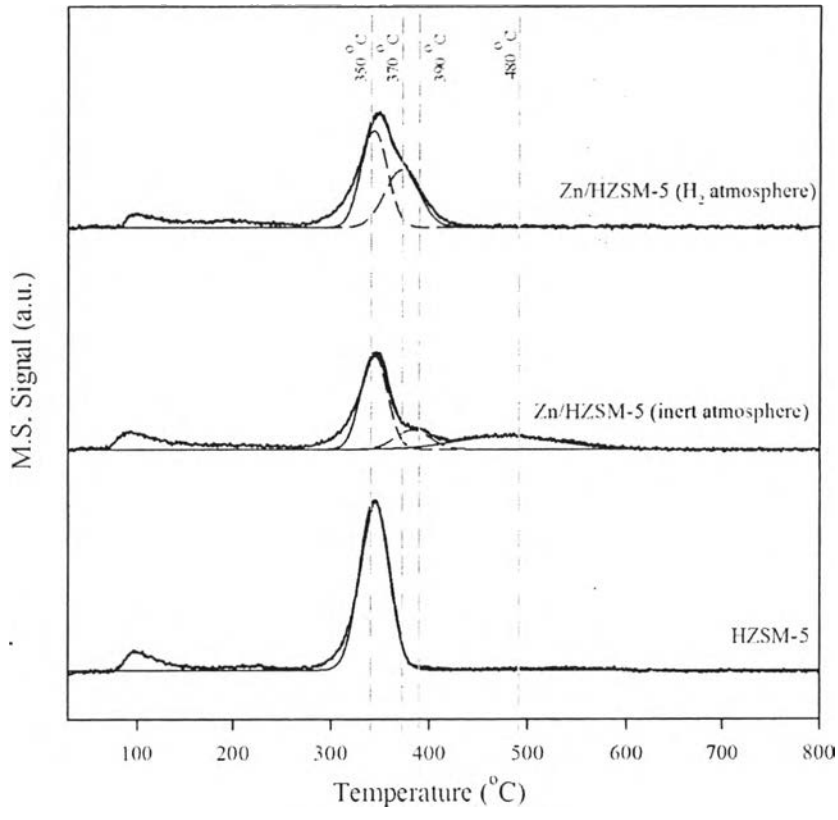

Figure 6.2 Isopropylamine–TPD (IPA–TPD) profiles of HZSM–5, Zn/HZSM–5 investigated under inert and H_2 atmospheres. The mass monitored was propylene (*m/e* = 41).

Table 6.2 Acidic properties of HZSM–5 and Zn/HZSM–5 catalysts investigated under inert and H_2 atmospheres

Catalysts	Brønsted acidity (μmol/g) [a]				
	350 °C	370 °C	390 °C	480 °C	Total
HZSM–5	373	–	–	–	373
Zn/HZSM–5 (inert atmosphere)	189	–	52	102	343
Zn/HZSM–5 (H_2 atmosphere)	194	152	–	–	346

[a] The data were calculated from IPA–TPD curves (propylene, *m/e* = 41).

As a result, $(ZnH)^+$ species was generated at the exchangeable sites following equation 2.

$$(AlO_2)^- (ZnOH)^+ + H_2 \rightarrow (AlO_2)^- (ZnH)^+ + H_2O \qquad (2)$$

Accordingly the strength of acid sites previously interact with the $(ZnOH)^+$ would be modified. This hypothesis was also confirmed by the quantitative analysis of desorbed propylene (*m/e* = 44), as shown in Table 6.2. The amount of the new Brønsted acid sites at 370 °C (152 μmol/g_{cat}) approximately equal to the summation of those at 390 °C (52 μmol/g_{cat}) and 480 °C (102 μmol/g_{cat}). The increase in acid strength of such acid site is in line with the higher electronegative nature of the new $(ZnH)^+$ species, as compared to the $(ZnOH)^+$ species.

One could dispute that instead of forming $(ZnH)^+$ species, the hydrogen treated Zn/HZSM–5 catalyst might lead to the complete reduction of the $(ZnOH)^+$ species to metallic Zn. However the formation of metallic Zn would result in the increase in total Brønsted acidity, which is in contrast with the IPA–TPD results (Table 6.2). A comparable total Brønsted acidity over the Zn/HZSM–5 operated under both inert (343 μmol/g) and H_2 (346 μmol/g) atmospheres was observed, confirming the absence of metallic Zn species upon reduction.

6.4.3 Analysis of Zn Species

The analysis spectra of Zn species using X–ray photoelectron spectroscopy (XPS) are exhibited in Fig. 6.3. Compared to the standard ZnO (Fig. 6.3a), the Zn ($2p_{3/2}$) XPS spectrum of the as–prepared Zn/HZSM–5 catalyst showed a higher binding energy at 1024.1 eV (Fig. 6.3b), attributed to $(ZnOH)^+$ species [26]. The hypsochromic shift was a result from Zn^{2+} interacting with the electronegative oxygen framework [35, 36]. Near–edge X–ray absorption spectrum at the Zn K–edge of the as–prepared Zn/HZSM–5 catalyst compared to standard ZnO and metallic Zn are illustrated in Fig. 6.4. The XANES spectrum of ZnO can be taken as a standard of tetrahedrally coordinated Zn species whereas the increased white line and the decreased edge widths in as–prepared Zn/HZSM–5 catalyst is dedicated to the presence of octahedrally coordinated Zn. The change from tetrahedral to octahedral coordination can be explained by the existing of hydrated shell around the

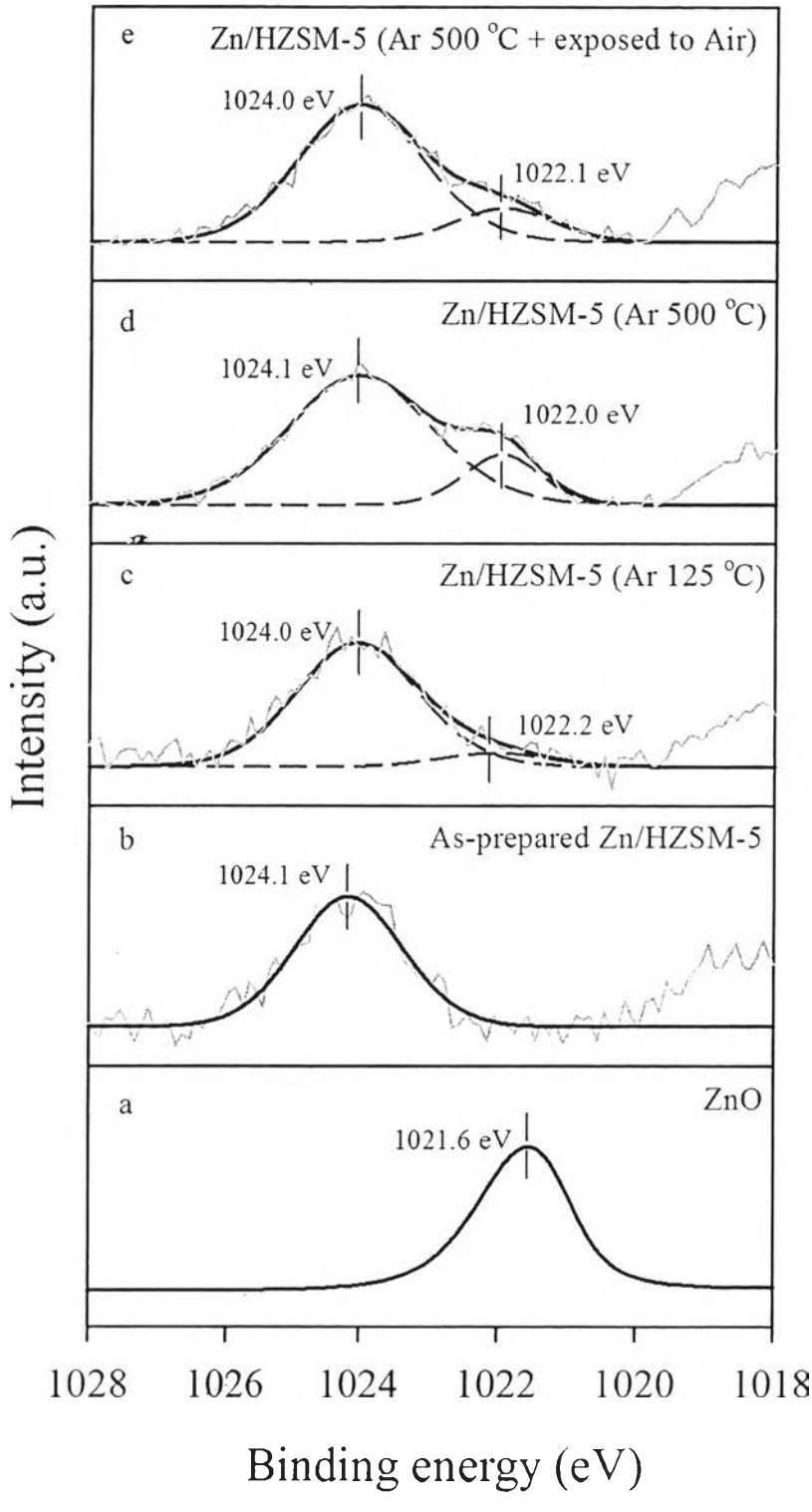

Figure 6.3 XPS (Zn ($2p_{3/2}$)) spectra of standard ZnO (a), As–prepared Zn/HZSM–5 (b), Zn/HZSM–5 catalysts treated under inert atmosphere at 125 °C (c), 500 °C (d), and 500 °C following with exposed to atmosphere at room temperature for 1 h (e).

Zn ion at the exchangeable sites [37]. The results confirmed that most of the Zn species in as–prepared catalyst appeared as isolated cationic species, presumably $(ZnOH)^+$ [33].

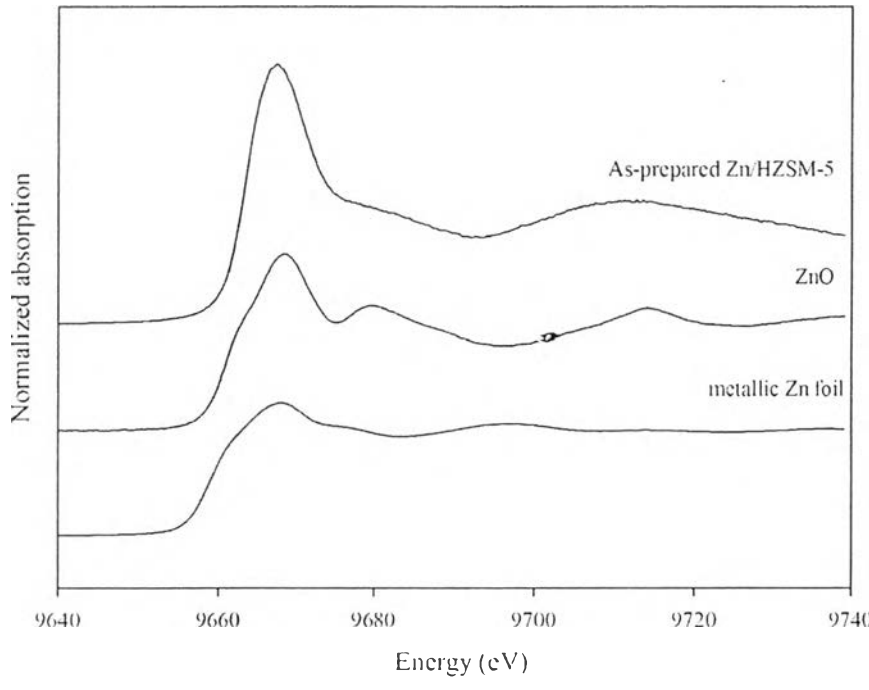

Figure 6.4 Zn K–edge X–ray absorption near edge structures of metallic Zn foil, ZnO, and As–prepared Zn/HZSM–5 catalyst at room temperature.

In order to identify Zn species existing upon the reaction condition, the XPS was performed on the Zn/HZSM–5 treated under inert gas or H_2 atmospheres. After heating the Zn/HZSM–5 catalyst under inert atmosphere up to 125 °C (Fig. 6.3c), a new peak at the binding energy around 1022.2 eV was emerged and become more pronounced upon heating to 500 °C (Fig. 6.3d). This new peak at lower binding energy (1022.2 eV) was dedicated to the exchangeable Zn^{2+} species, generated by the dehydroxylation of $(ZnOH)^+$ species with a proximated Brønsted acid site, i.e. via the reversion of equation 1. The decrease in the binding energy of Zn^{2+}, as compared to $(ZnOH)^+$ inferred that the Brønsted acid site, previously interacted with the $(ZnOH)^+$ species was disappeared upon dehydroxylation to Zn^{2+} species. Despite increasing temperature to the reaction condition (500 °C, Fig 6.3d),

the $(ZnOH)^+$ (peak at 1024.1 eV) was the dominant zinc species in the sample. It is worth to emphasize that in our case, Zn cations were exchanged with HZSM–5 catalyst that has the Si/Al ratio of 15. The high Si/Al ratio implied that the opportunity that Zn cations will locate as Zn^{2+} on two adjacent Al centers is very low. Therefore, only small part of the exchangeable Zn^{2+} was formed at the reaction temperature while the majority remained as $(ZnOH)^+$ species. One might suggest that the dehydroxylation of $(ZnOH)^+$ species could occur by reacting with the neighbor $(ZnOH)^+$, forming $2(AlO_2)^-$ $(ZnOZn)^{2+}$ [14, 18] as shown in equation 3. However, the formation of $2(AlO_2)^-$ $(ZnOZn)^{2+}$ species shall not be generated over the high Si/Al sample with relatively low Zn content, prepared by aqueous phase ion–exchange method [26, 38]. According to our previous work [30], the TPR, XPS, and EXAFS results also confirmed the inexistence of this $2(AlO_2)^-$ $(ZnOZn)^{2+}$ species.

$$(AlO_2)^- (ZnOH)^+ + (AlO_2)^- (ZnOH)^+ \rightarrow 2(AlO_2)^- (ZnOZn)^{2+} + H_2O \qquad (3)$$

By exposing the thermal treated Zn/HZSM–5 (Ar 500 °C) to atmosphere at room temperature for one hour, the exchangeable Zn^{2+} species would promptly react with water from the humid air, regenerating $(ZnOH)^+$ species. Accordingly, some of the $(ZnOH)^+$ species was recovered as seen by an increase in the intensity of the peak at 1024 eV, together with a proportional decrease within the intensity of the peak at 1022 eV as illustrated in Fig. 6.3e.

The effect of hydrogen to the evolution of zinc species was also investigated as illustrated in Fig. 6.5. After treating the catalyst under hydrogen flow at 150 °C for 1 h, the XPS spectrum of Zn/HZSM–5 (Fig. 6.5b) showed the peak of the remaining $(ZnOH)^+$ at 1024.1 eV and the new peak at 1023.5 eV. The appearance of lower binding energy peak was dedicated to the $(ZnH)^+$ species, generated by the hydrodehydroxylation of $(ZnOH)^+$ species, as in equation 2. This explanation was in agreement with the theoretical studies showing that $(ZnOH)^+$ was transformed by accepting the H from ethane molecules and releasing water as a product [39]. The decrease in binding energy of $(ZnH)^+$ species was resulted from

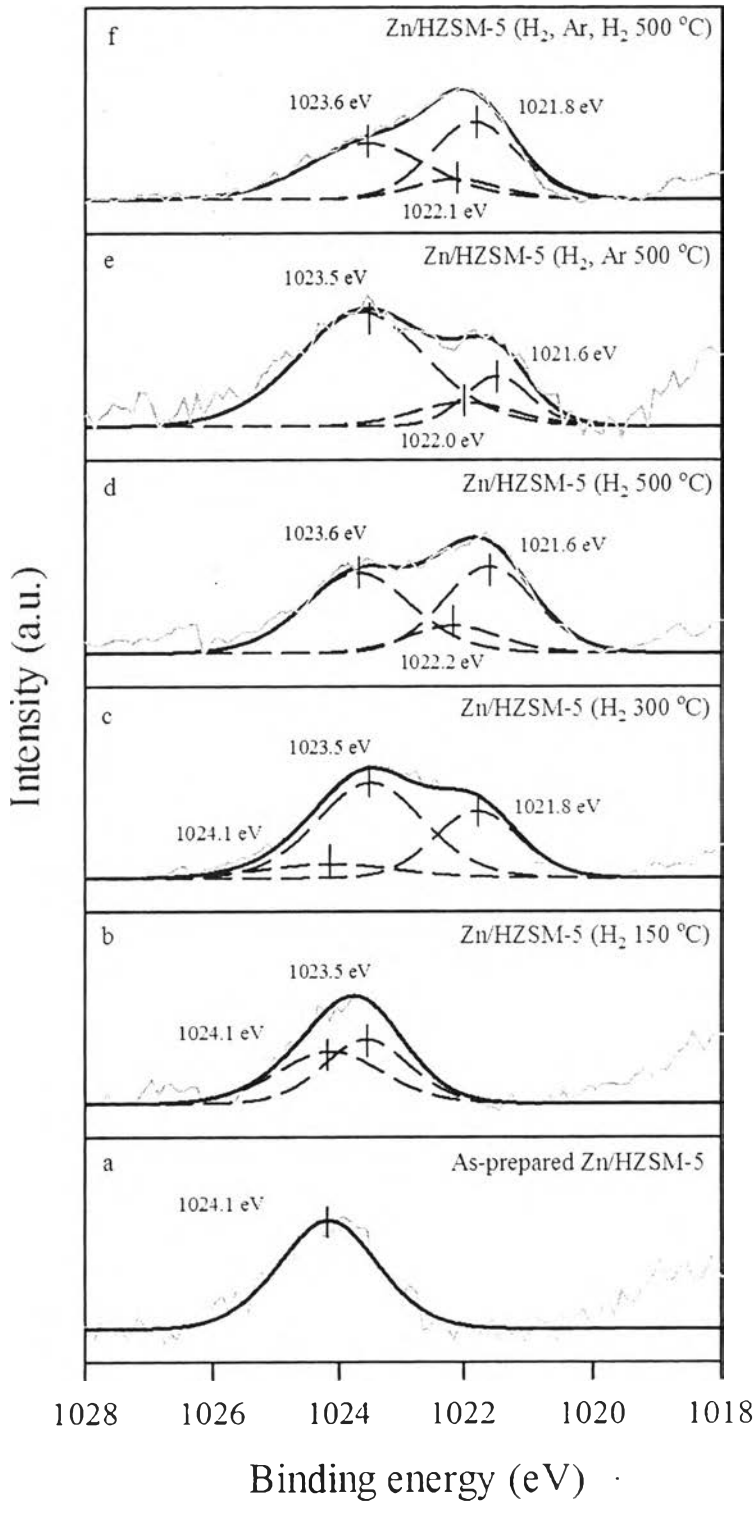

Figure 6.5 XPS (Zn ($2p_{3/2}$)) spectra of as–prepared Zn/HZSM–5 (a), Zn/HZSM–5 after different treatments; for 1 h under H_2 at 150 °C (b), H_2 at 300 °C (c), H_2 at 500 °C (d) following with Ar at 500 °C (e), and H_2 at 500 °C (f).

the lower electronegativity of dissociated hydrogen atoms compared with oxygen of the hydroxyl group. After further heating the catalyst to 300 °C (Fig. 6.5c), a nearly complete transformation of $(ZnOH)^+$ species was clearly noticed. At this temperature, the results showed not only a significant increase of $(ZnH)^+$ species (1023.5 eV) but also the formation of new peak at 1021.8 eV. The lower binding energy peak illustrated that this new active Zn species possessed the lower electron affinity as compared with $(ZnH)^+$ species. The formation of this Zn species might be explained by the chemisorption of another hydrogen molecule on the $(ZnH)^+$ species, resulting in the formation of $(ZnH_3)^+$ species. The dissociation of H_2 molecule on the exchangeable cationic center was widely studied in the case of Ga^+ species. In that case, the dihydrido gallium species $(GaH_2)^+$ was generated and could be stabilized only under hydrogen atmosphere [40, 41].

At 500 °C, the deconvolution of XPS spectrum exhibited the complete disappearance of $(ZnOH)^+$ species (Fig. 6.5d). The dominant of $(ZnH_3)^+$ over $(ZnH)^+$ species suggested that $(ZnH_3)^+$ was formed with the expense of $(ZnH)^+$ species. It should be emphasized that the evolution of $(ZnOH)^+$ to $(ZnH)^+$ and $(ZnH_3)^+$ species only occurred on the bivalent Zn cation, stabilized on isolated one Al center. On the other hand, in the case of exchangeable Zn^{2+} located on two Al centers $(2(AlO_2)^-Zn^{2+})$, even the dissociation of hydrogen was formed, generating $(ZnH)^+$ and recovered Brønsted acid site, the recombinative desorption of hydrogen between $(ZnH)^+$ species and H^+ of recovered Brønsted acid site can also occur easily. That led to the remaining of the exchangeable Zn^{2+} species. As proved by XPS, the exchangeable Zn^{2+} species was observed as a minor part at 1022.2 eV, agreed very well with the XPS spectrum of Zn/HZSM–5 catalyst heated under inert atmosphere at the same temperature (Fig 6.3d). The stability upon the absence of H_2 of $(ZnH_3)^+$ species was further studied by switching the treating gas from H_2 to Ar and heating at 500 °C for 1 h (Fig. 6.5e). The significant decrease of $(ZnH_3)^+$ species (1021.6 eV) was detected with the increase of the $(ZnH)^+$ species (1023.6 eV). Notwithstanding, the regeneration of $(ZnH_3)^+$ species was observed again after introducing of H_2 (Fig. 6.5f), suggesting that the process is reversible depending on H_2 atmosphere. This is in a manner similar to the formation of $(GaH_2)^+$ as mentioned earlier.

One might argue that heating under hydrogen atmosphere could lead to the complete reduction of bivalent Zn cations thus the lowest binding energy peak (approximately 1021.6 eV) might be the metallic Zn^0. This assumption was excluded due to the comparable amount of Brønsted acidity of Zn/HZSM–5 treated with and without hydrogen as formally confirmed by IPA–TPD (Table 6.2). Moreover, the reversibility between both two reductive Zn species ($(ZnH)^+$ and $(ZnH_3)^+$) in the absence of oxidizing agent (Fig 6.5d, e, f) also ensured the same oxidation state of the Zn species, but different in number of the hydrogen–incorporated.

6.4.4 The Dependence of Aromatization Activities on $(ZnOH)^+$ and ZnH^+ Species

The effect of Zn species on *n*–pentane aromatization was studied in a pulse mode under He atmosphere. The HZSM–5 and Zn/HZSM–5 catalysts were treated with and without H_2 prior to introducing the pulse of *n*–pentane. As shown in Table 6.3, 19 % conversion of *n*–pentane with 11 % and 34 % selectivity of BTX aromatics and paraffins were respectively obtained over the parent HZSM–5 catalyst. Without the H_2 treatment, Zn/HZSM–5 catalyst showed a lower conversion (14 %), but higher BTX aromatics selectivity (22 %) with the decrease in paraffins selectivity (18 %). As widely accepted [26, 30, 42], the dehydrogenation activity of $(ZnOH)^+$ species reinforced the transformation of light paraffins to olefins, resulting in low paraffins and high aromatics formations.

The catalytic activity of the reduced Zn species was tested by heating Zn/HZSM–5 catalyst under the H_2 atmosphere for 1 h, denoted as Zn/HZSM–5 (H_2 Treatment). Although, a similar conversion was observed with non–reduced Zn species, the results showed that the BTX aromatics selectivity remarkably increased from 22 % to 31 %. To confirm that the significant increase in aromatics selectivity was a result from the presence of zinc, parent HZSM–5 catalyst was also treated under H_2. As expected, a comparable product distribution was detected over both treated and untreated HZSM–5 catalysts.

Table 6.3 Product distribution of *n*–Pentane transformation over HZSM–5 and Zn/HZSM–5 catalysts with and without the H_2 pre–treatment

Product distribution (wt %)	Catalysts			
	HZSM–5	HZSM–5 (H_2 Treatment)	Zn/HZSM–5	Zn/HZSM–5 (H_2 Treatment)
Conversion	**19**	**20**	**14**	**16**
Product selectivity				
Paraffins	**34**	**34**	**18**	**16**
Methane	3	3	3	2
Ethane	12	11	8	8
Propane	15	14	7	6
Butane	4	5	0	0
Olefins	**55**	**55**	**60**	**52**
Ethylene	22	22	25	23
Propylene	28	28	32	27
Butene	5	5	3	2
BTX aromatics	**11**	**11**	**22**	**31**
Benzene	4	4	7	10
Toluene	5	5	10	14
Xylenes	2	2	5	7

Regarding the Zn/HZSM–5 catalyst with H_2 treatment, the dehydrogenation over the reduced Zn species ($(ZnH_3)^+$ or $(ZnH)^+$) could occur via the heterolytic dissociation of C–H bond. It is likely that the carbocation would interact with oxygen bridge while the H interacts with the Zn species. This leads to a

reductive elimination of the hydrido complex bearing hydrogen gas while the active Zn species was recovered by the H–transfer from the carbocation yielding an olefin [25].

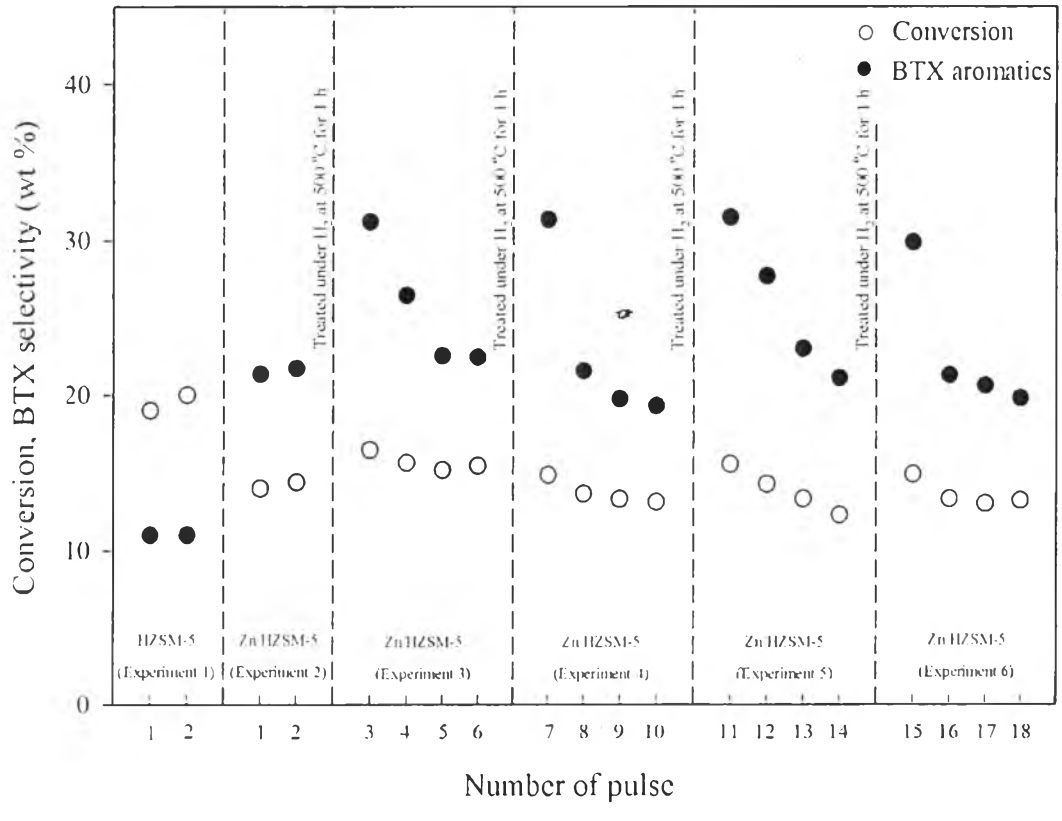

Figure 6.6 *n*-Pentane conversion and BTX selectivity over HZSM-5 and Zn/HZSM-5 catalysts with different treatments. Reaction conditions: atmospheric pressure, 500 °C, catalyst = 50 mg, 0.025 mL of *n*-pentane gas, 180 mL/min of He.

In order to clearly understand the catalytic activity of $(ZnH)^+$ species, the cycles of H_2 treatment and catalytic activity testing were investigated as shown in Fig. 6.6. When Zn/HZSM–5 catalyst was treated with H_2 (Experiment 3), selectivity of BTX is increased by approximately 10 %. However, it was declined within 3–4 pulses of *n*–pentane. By re–treating Zn/HZSM–5 catalyst (Experiments 4, 5, 6), aromatics selectivity was increased again. The similar results can be repeatedly observed, implying that the active species is not stable. It is worth noting that the

aromatics selectivity of treated Zn/HZSM–5 catalyst finally dropped to the same level as untreated Zn/HZSM–5 catalyst. Nonetheless, the absence of water during the reaction confirmed that $(ZnOH)^+$ species was unable to be regenerated.

According to above observation, it is likely that the active species, that gives high selectivity to BTX at the first pulse, is the $(ZnH_3)^+$ formed during H_2 treatment. As H_2 is removed, the $(ZnH_3)^+$ is decomposed under inert, presumably to $(ZnH)^+$ and H_2, as observed by XPS (Fig. 6.5e). However, the active $(ZnH_3)^+$ species could be reproduced upon re–treating with H_2 The $(ZnH)^+$ species is also active for *n*–pentane aromatization, but in a less extent as compared to the $(ZnH_3)^+$ species. The results led to the conclusion that compared with $(ZnOH)^+$, $(ZnH_3)^+$ and $(ZnH)^+$ species perform the higher catalytic activity in aromatization of *n*–pentane.

6.5 Conclusion

In this work, we explored the evolution of Zn species over Zn/HZSM–5 catalysts by using the thermal treatment under inert or hydrogen atmospheres. The effects of each Zn species to the aromatization of *n*–pentane were revealed. By using aqueous phase ion–exchange method, only $(ZnOH)^+$ species was found in as–prepared Zn/HZSM–5 catalyst. Under the reaction temperature, most of Zn species stabilized in the form of isolated $(ZnOH)^+$ while a minor part of $(ZnOH)^+$ combined with the neighboring hydroxyl group and created the exchangeable Zn^{2+} species. The conventional $(ZnOH)^+$ showed the improvement in the aromatization activity as agreed in previous studies. Nonetheless by introducing the hydrogen treatment, the hydrodehydroxylation of $(ZnOH)^+$ generated the new active $(ZnH)^+$ and $(ZnH_3)^+$ species. The remarkable increase in aromatics selectivity was noticed, illustrating the higher aromatization activity of $(ZnH)^+$ and $(ZnH_3)^+$ species, as compared with the conventional $(ZnOH)^+$ species. However, under the absence of H_2, the most active species, $(ZnH_3)^+$, decomposed to $(ZnH)^+$, resulting in a somewhat lower the aromatization activity. Even though the $(ZnH_3)^+$ was unstable in the absence of H_2, it could be reproduced upon H_2 treatment.

6.6 Acknowledgements

The authors are grateful for the financially supported by the Center of Excellence on Petrochemical and Materials Technology and the Petroleum and Petrochemical College, Chulalongkorn University, Thailand. The help in XANES measurement was provided by BL8, Synchrotron Light Research Institute (SLRI), Thailand.

6.7 References

1 Y. Ono, Catal. Rev. Sci. Eng. 34 (1992) 179

2 P. Dejaifve, A. Aurou, P.C. Gravelle, J.C. Vedrine, J. Catal. 70 (1981) 123.

3 T. Inui, Y. Makino, F. Okazumi, S. Nagano, A. Miyamoto, Ind. Eng. Chem. Res. 26 (1987) 647.

4 P. Meriaudeau, G. Sapaly, C. Naccache, Stud. Surf. Sci. Catal. 49 (1989) 1423.

5 R.L.V. Mao, L. Dufresne, Appl. Catal. 52 (1989) 1.

6 C.D. Gosling, F.P. Wilcher, L. Sullivan, Hydrocarbon Process. 12 (1991) 69.

7 G. Giannetto, R. Monque, R. Galiasso, Catal. Rev. Sci. Eng. 36 (1994) 271.

8 D. Seddon, Catal. Today 6 (1989) 351.

9 I. Inui, F. Okazumi, J. Catal. 90 (1984) 366.

10 Y. Ono, K. Kanae, J. Chem. Soc. Faraday Trans. 87 (1991) 669.

11 L.Yu, S. Huang, S. Zhang, Z. Liu, W. Xin, S.Xie, L. Xu, ACS Catal. 2 (2012) 1203.

12 T. Mole, J.R. Anderson, G. Creer, Appl. Catal. 17 (1985) 141.

13 E. Iglesia, J.E. Baumgartner, Catal. Lett. 21 (1993) 55.

14 H. Berndt, G. Lietz, B. Lucke, J. Volter, Appl. Catal. 146 (1996) 351.

15 H. Berndt, G. Lietz, J. Volter, Appl. Catal. 146 (1996) 365.

16 E. Iglesia, J.E. Baumgartner, G.L. Price, J. Catal. 134 (1992) 549.

17 A. Hagen, F. Roessber, Catal. Rev. Sci. Eng. 42 (2000) 403.

18 J.A. Biscardi, E. Iglesia, J. Phys. Chem. B 102 (1998) 9684.

19 S.M.T. Almutairi, B. Mezari, P.C.M.M. Magusin, E.A. Pidko, E.J.M. Hensen, ACS Catal. 2 (2011) 71.

20 J.A. Biscardi, E. Iglesia, Catal. Today 31 (1996) 207.

21 J.A. Biscardi, E. Iglesia, J. Catal. 182 (1999) 117

22 J.A. Biscardi, G.D. Meitzner, E. Iglesia, J. of Catal. 179 (1998) 192.

23 S.Y. Yu, J.A. Biscardi, E. Iglesia, J. Phys. Chem. B 106 (2002) 9642.

24 L.M. Lubango, M.S. Scurrell, Appl. Catal. A 235 (2002) 265.

25 H.A. Aleksandrov, G.N. Vayssilov, Catal. Today 152 (2010) 78.

26 X. Niu, J. Gao, Q. Miao, M. Dong, G. Wang, W. Fan, Z. Qin, Microporous and Mesoporous Mater. 197 (2014) 252.

27 H.A. Aleksandrov, G.N. Vayssilov, N. Rosch, J. Mol. Catal. A-Chem 256 (2006) 149.

28 S. Triwahyono, A.A. Jalil, R.R. Mukti, M. Musthofa, N.A.M. Razali, M.A.A. Aziz, Appl. Catal. A 407 (2011) 91.

29 L.A.M.M. Barbosa, R.A.V. Santen, J. Phys. Chem. C 111 (2007) 8337.

30 S. Tamiyakul, W. Ubolcharoen, D.N. Tungasmita, S. Jongpatiwut. Catal. Today 256 (2015) 325.

31 T.J.G. Kotke, R.J. Gorte, G.T. Kokotailo, W.E. Farneth, J. Catal. 115 (1989) 265.

32 A. Ausavasukhi, T.Sooknoi, D.E. Resasco, J. Catal. 268 (2009) 68.

33 El-M. El-Malki, R.A. van Santen, W.M.H. Sachtler, J. Phys. Chem. B 103 (1999) 4611.

34 L.A.M.M. Barbosa, R.A.V. Santen, Catal. Lett. 63 (1999) 97.

35 J. Chen, L. Zhang, H.M. Kang, F.X. Ding, Chin. J. Catal. 22 (2001) 229.

36 J. Chen, Z. Feng, P. Ying, C. Li, J. Phys. Chem. B 108 (2004) 12669.

37 A. Hagen, K.H. Hallmeier, C. Henning, R. Szargan, T. Inui, F. Roessner, Stud. Surf. Sci. Catal. 94 (1995) 195.

38 G. Engelhardt, in troduction to Zeolite Science and Technology, ed. H. van Bekkum, E.M. Flaningen and J.C. Jansen, Elsevier, Amsterdam, 1991, ch. 8, pp. 285-315

39 A.L. Yakovlev, A.A. Shubin, G.M. Zhidomirov, R.A. van Santen, Catal. Lett. 70 (2000) 175.

40 A. Ausavasukhi, T. Sooknoi, Catal. Commun. 45 (2014) 63.

41 V.B. Kazansky, I.R. Subbotina, R.A. van Santen, E.J.M. Hensen, J. Catal. 233

(2005) 351.

42 S. tamiyakul, S. Anutamjarikun, S. Jongpatiwut, Catal. Commun. 74 (2016) 49.